DEFORMATION ANALYSIS OF EMBANKMENTS

By N. Loganathan,[1] A. S. Balasubramaniam,[2] Fellow, ASCE, and D. T. Bergado,[3] Associate Member, ASCE

ABSTRACT: Settlement and stability are the primary geotechnical considerations in the design of embankments founded on soft clay. Settlements are inevitably associated with lateral deformations. Lateral flow in turn is an indirect measure of the stability of embankments. Therefore, a detailed study of different settlement components and lateral deformations and their correlations will provide guidelines for an embankment design. This paper presents a new methodology, termed "Field Deformation Analysis (FDA)," which is based on a simple concept dealing with lateral and vertical deformation characteristics of soft foundations under embankment stage loading. This method is used to delineate and quantify different settlement components, namely, immediate settlement, consolidation settlement, and creep settlement, from the total settlement measured during field observations, for the loading and consolidation stages. Finite element method (FEM) of analysis was performed for comparison with FDA results. The FEM analysis was performed using the CRISP computer program, developed at Cambridge University, which uses many soil constitutive models including the modified Cam-clay model. In 1988, the Malaysian Highway Authority was authorized to build 13 full-scale test embankments at Muar Flats, of which two were constructed without any foundation ground improvements. A comparison study of the results from FDA and FEM, performed for both the untreated full-scale test embankments, revealed very good agreement during loading and consolidation stages. In addition, a consistent relationship between the different settlement components was also observed during the different stages of embankment loading.

INTRODUCTION

The total settlement observed beneath an embankment subjected to step loading, is basically a combination of different components, namely, immediate settlement, consolidation settlement, and creep settlement. Establishing relationships among these settlements components, upon separating them from the total settlement observed in the field, will facilitate settlement predictions from relatively simple numerical computations. The separation of settlement components provides better understanding of settlement mechanism and thus far better design of step loading. In addition, it helps for the selection of appropriate ground-improvement method.

An extensive numerical analysis, using FEM, was performed by Christian and Watt (1972) to delineate and quantify different settlement components. The elasto-viscoplastic constitutive model was used for the foundation soil in their analysis. Time-dependent deformations due to undrained creep can be quite large in both normally consolidated and highly overconsolidated clays. Creep effects are more important for horizontal than for vertical deformations (Christian and Watt 1972). However, coupling of drained

[1]Geotech. Engrg., Geo-Envir. Sdn. Bhd., Suite 804, IGB Plaza, 6 Jalan Kampar, 50400 Kuala Lumpur, Malaysia.

[2]Prof. of Geotech. Engrg., Geotech. and Transp. Engrg. Div., Asian Inst. of Tech., Bangkok, Thailand.

[3]Assoc. Prof. of Geotech. Engrg., Geotech. and Transp. Engrg. Div., Asian Inst. of Tech., Bangkok, Thailand.

Note. Discussion open until January 1, 1994. To extend the closing date one month, a written request must be filed with the ASCE Manager of Journals. The manuscript for this paper was submitted for review and possible publication on June 9, 1992. This paper is part of the ***Journal of Geotechnical Engineering***, Vol. 119, No. 8, August, 1993. ©ASCE, ISSN 0733-9410/93/0008-1185/$1.00 + $.15 per page. Paper No. 4221.

creep with the undrained one could be analytically more cumbersome and would require soil data that are difficult to obtain.

A new methodology, termed as field deformation analysis (FDA), based on the changes in volume of foundation soil under embankment loading, is proposed in this paper to separate and quantify settlement components. An extensive FEM analysis is also performed for purposes of verification of results obtained from FDA. Shibata (1987) observed that significant volume changes occur during embankment construction and that the behavior of the embankment deviated significantly from undrained conditions. Ting et al. (1989) and Toh et al. (1989) used a similar concept, considering volumetric deformation of embankment foundation under loading, to separate settlement components for Malaysian embankments. However, proper theoretical formulation of this volumetric deformation concept is not available to date. In this paper, an attempt is made to formulate this concept. The validity of the formulation is confirmed from a comparison study performed with results obtained from FEM analysis.

TEST EMBANKMENTS AT MUAR FLATS

A total of 13 full-scale field-test embankments, nine 6-m high and four 3-m high, were authorized for construction at a section of the express highway that is located at Muar Flat in the valley of the Muar River by the Malaysian Highway Authority (MHA). Nine different methods of ground improvement were used to study the effectiveness of each method. Two embankments, one 6-m high (171 m $\times$ 50 m in plan—scheme 6/6 in Fig. 1) and one 3-m high (50 m $\times$ 32 m in plan—scheme 3/2 in Fig. 1), were constructed without any ground treatment for comparison. The locations of these embankments are shown in Fig. 1.

In addition, a conventional embankment, without any treatment or berm, was also built with increasing height until failure was reached. The performance of this embankment, especially pore pressure pattern, stability, settlement, and lateral deformation, were predicted by four predictors, namely, Prof. A. S. Balasubramaniam (Thailand), Prof. J. P. Magnan (France), Prof. A. Nakase (Japan), and Prof. H. G. Poulos (Australia). Their predictions were presented in the "International Symposium on Trial Embankments on Malaysian Muar Clays," in November 1989, held in Kuala Lumpur, Malaysia. All predictors were given the same soil properties and field instrumentation results (Brand and Premchitt 1989).

The subsurface exploration program included: (1) Wash borings; (2) undisturbed sampling using stationary thin wall piston samplers with internal diameters of 72 mm and 140 mm; (3) vane shear test; (4) piezocone test; and (5) installation of various instruments to monitor the field performances. The locations of boreholes and the in situ testing are also shown in Fig. 1. The soil testing program was carried out in three phases by the Malaysian Highway Authority (MHA) and the Asian Institute of Technology (AIT), Thailand. The soil profile at the location of trial is presented in Fig. 2(*a*). A weathered crust with secondary laterite concentrations and mottles extended approximately 1.5 m below the ground surface. Below this soft greenish gray silty clay lies the upper clay underlain by the lower clay (from 7 m to 20 m), which continues down up to 6-m depth. The water content, Atterberg limits, vane shear strength, and Dutch cone resistance profiles with the depth are shown in Fig. 2(*b*). The complete soil properties of Malaysian Muar clay was summarized by Brand and Premchitt (1989).

TYPES OF S.I. WORK		PHASE I	PHASE II	PHASE III
BOREHOLE	BH	BH1 TO BH2	KSBH1 - KSBH2	KSBH3 - KSBH4 BH3 - BH7 SSP BH1 - SSPBH2
PISTON SAMPLING	PS	PS1 TO PS2	PS3 TO PS11	PS12
IN-SITU VANE SHEAR TESTS	GV	GV1 TO GV9	KSGV1 - KSGV2	KSGV3 TO KSGV5 GV10 TO GV25
STATIC CONE PENETRATION TESTS (PIEZOCONE)	CPT	CPT1 TO CPT4	–	SSP CPT1 - SSP CPT4 CPT5 - CPT15
STATIC CONE PENETRATION TESTS(MECHANICAL CONE)	DS	–	–	DS1 TO DS14

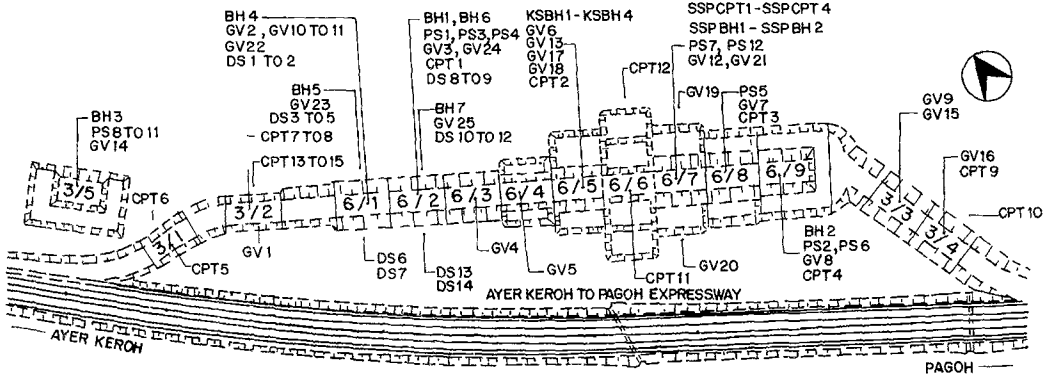

FIG. 1. Locations of Trial Embankments and Subsurface Explorations

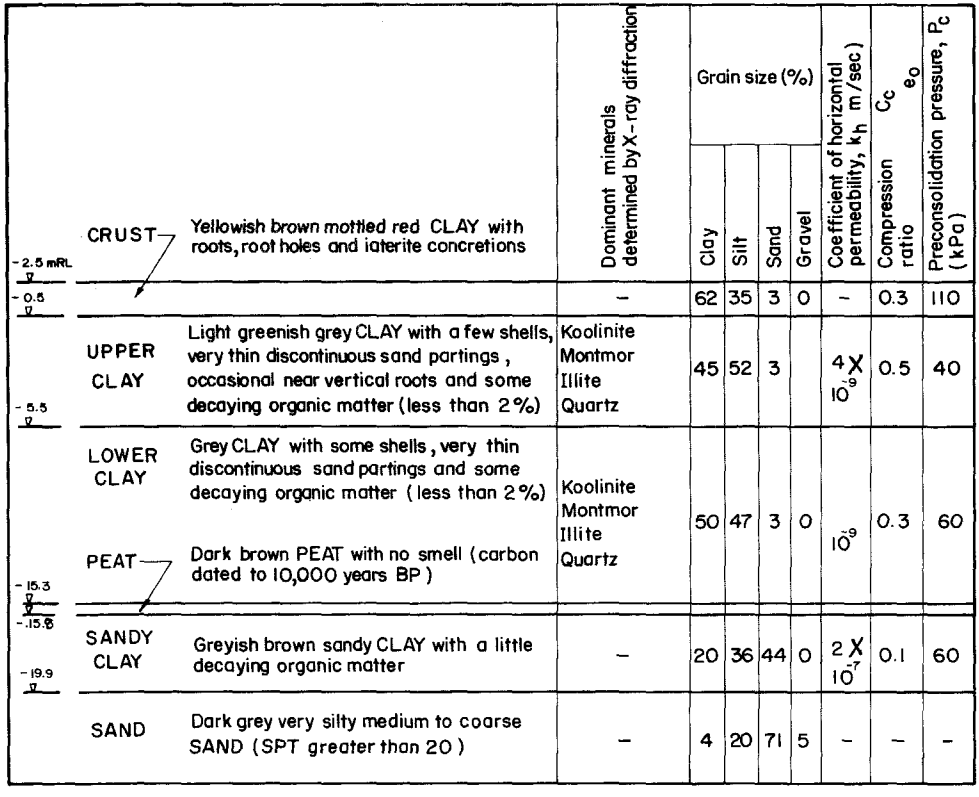

FIG. 2. Typical Subsurface Profile at Site

FIELD DEFORMATION ANALYSIS (FDA)

Theory

During loading and consolidation stages of an embankment subjected to step loading, considerable volume changes occur in the foundation soil, the magnitude of which depend upon the load applied and the duration of consolidation. The volume changes, which occur vertically and laterally, are associated with settlements and lateral deformations of an embankment foundation. Undrained settlements occur without any changes in net volume and therefore the settlement volume is the same as the lateral volume, provided that the soil is fully saturated. Lateral and vertical volume changes in an embankment foundation vary in different ways during the consolidation stage as in the pattern of pore-pressure dissipation. Therefore, the settlement components can be separated for both loading and consolidation stages using the volume-change concept.

Loading Stage

The total settlement observed during loading is a combination of immediate and consolidation settlement components. Fig. 3 shows the subsoil deformation pattern due to undrained deformation, which causes the immediate settlement. Since this occurs in an undrained manner, the magnitude of settlement deformation volume, designated as AOC, should be equal to the lateral deformation volume, designated as APM. Due to dissipation of excess pore pressures, the process of consolidation takes place simultaneously. Fig. 3 also shows the ultimate deformation pattern of the embankment foundation at the end of loading, where the volume changes vertically (ABC) and laterally ($APMQA$) are due to consolidation. It

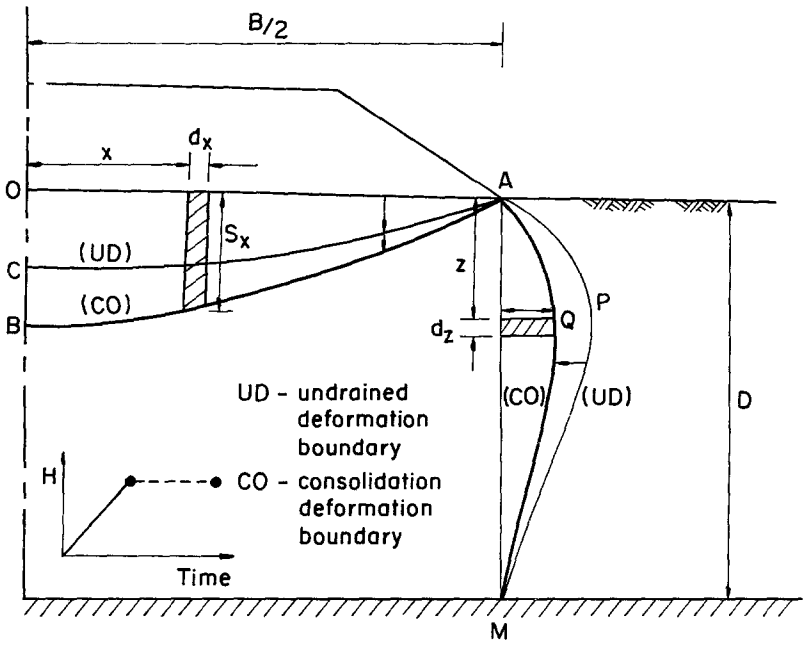

FIG. 3. Deformation Pattern of Embankment Foundation at End of Loading Stage

should be noted that the volumes referred to here are for the unit length of the embankment.

The volume change due to settlement of an embankment foundation can be computed from the field measurements of settlement gauges as in (1).

$$V_{vL} = \int_0^{B/2} \rho_x \cdot dx \quad \ldots\ldots (1)$$

where V_{vL} = the observed settlement volume in the field from settlement gauge readings, for half the embankment; ρ_x = settlement at a distance x from the centerline of the embankment, and B = the width of the embankment.

The settlement volume V_{vL} at the end of each loading stage is the resultant of the volume change due to the immediate settlement (V_{iL}) and the consolidation settlement (V_{cL}) as shown in Fig. 3. Since the loading period is comparatively small, the creep settlement is ignored. Therefore

$$V_{vL} = V_{iL} + V_{cL} \quad \ldots\ldots (2)$$

The lateral volume increase due to undrained deformation (immediate settlement) decreases during consolidation due to the dissipation of excess pore pressures (Christian and Watt 1972). Let α be the ratio of the lateral volume reduction to the consolidation settlement volume

$$\alpha = \frac{\text{lateral consolidation volume}}{\text{consolidation settlement volume } (V_{cL})} \quad \ldots\ldots (3)$$

where the downward vertical displacement and the outward lateral movements are taken as positive. The lateral volume change at any time interval can be obtained by integrating the field measurements of the inclinometer installed at the toe of the embankment

$$V_{hL} = \int_0^D \delta_z \cdot dz \quad \ldots\ldots (4)$$

where V_{hL} = the observed lateral volume change in the field from inclinometer measurements, δ_z = the lateral deflection measured at the depth z, and D = the thickness of the soil stratum. The volume V_{hL} measured at the end of loading, is the resultant of lateral volume increase due to undrained deformation (V_{iL}—due to immediate settlement) and the lateral volume reduction during consolidation αV_{cL}).

$$V_{hL} = V_{iL} - \alpha V_{cL} \quad \ldots\ldots (5)$$

From (2) and (5), the volumetric deformation components of an embankment foundation (immediate and consolidation) during loading stage can be separated as given in (6) and (7).

$$V_{cL} = \frac{V_{vL} - V_{hL}}{1 + \alpha} \quad \ldots\ldots (6)$$

$$V_{iL} = \frac{\alpha V_{vL} + V_{hL}}{1 + \alpha} \quad \ldots\ldots (7)$$

It can be derived from elastic theory that the immediate settlement at the surface of a uniformly loaded flexible rectangular area is proportional to the load applied (Harr 1963).

$$\rho_i = \frac{\bar{B}(1 - \nu^2)I_3}{E} \cdot q \quad \ldots\ldots (8)$$

where $\bar{B}(1 - \nu^2)I_3/E$ = a constant for a given embankment and also it can be assumed that the load applied on embankment foundation is proportional to the height of the embankment (i.e., $q \propto H$), I_3 = the shape factor, and ν = the Poisson's ratio. Therefore it can be assumed for plane strain condition that the immediate settlement volume is linearly related to embankment height (i.e., $V_i = A \times H$, where A is a constant). For an embankment with staged construction the constant A can be evaluated at the end of each loading stage.

Stage j

$$A = \frac{(V_{iL})_j}{H_j} = \frac{\alpha \cdot \dfrac{(V_{vL})_j}{H_j} + \dfrac{(V_{hL})_j}{H_j}}{1 + \alpha} \quad \ldots\ldots (9)$$

Stage $j + 1$

$$A = \frac{(V_{iL})_{j+1}}{H_{j+1}} = \frac{\alpha \cdot \dfrac{(V_{vL})_{j+1}}{H_{j+1}} + \dfrac{(V_{hL})_{j+1}}{H_{j+1}}}{1 + \alpha} \quad \ldots\ldots (10)$$

Since A is a constant by (9) and (10) the value α can be obtained as given in (11)

$$\alpha = \frac{\left[\dfrac{(V_{hL})_{j+1}}{H_{j+1}} - \dfrac{(V_{hL})_j}{H_j}\right]}{\left[\dfrac{(V_{vL})_j}{H_j} - \dfrac{(V_{vL})_{j+1}}{H_{j+1}}\right]} \quad \ldots\ldots (11)$$

where (9), (10), and (11) assume the soil behaves as linear for given load increment.

Consolidation Stage

It is considered that the total settlement observed in the field during the consolidation stage is the resultant of consolidation settlement (ρ_c) and creep settlement (ρ_{cr}). The lateral consolidation volume ratio α and the lateral creep volume ratio β compared to their respective settlement volumes are assumed as:

$$\alpha = \frac{\text{lateral consolidation volume}}{\text{consolidation settlement volume } (V_{cC})} \quad \ldots\ldots (12)$$

$$\beta = \frac{\text{lateral creep volume}}{\text{creep settlement volume } (V_{crC})} \quad \ldots\ldots (13)$$

The volume change pattern during consolidation stage of an embankment is shown in Fig. 4. As derived for the loading stage, the volumes V_{vC} and V_{hC} can be written as (14) and (15).

$$V_{vC} = V_{cC} + V_{crC} \quad \ldots\ldots (14)$$

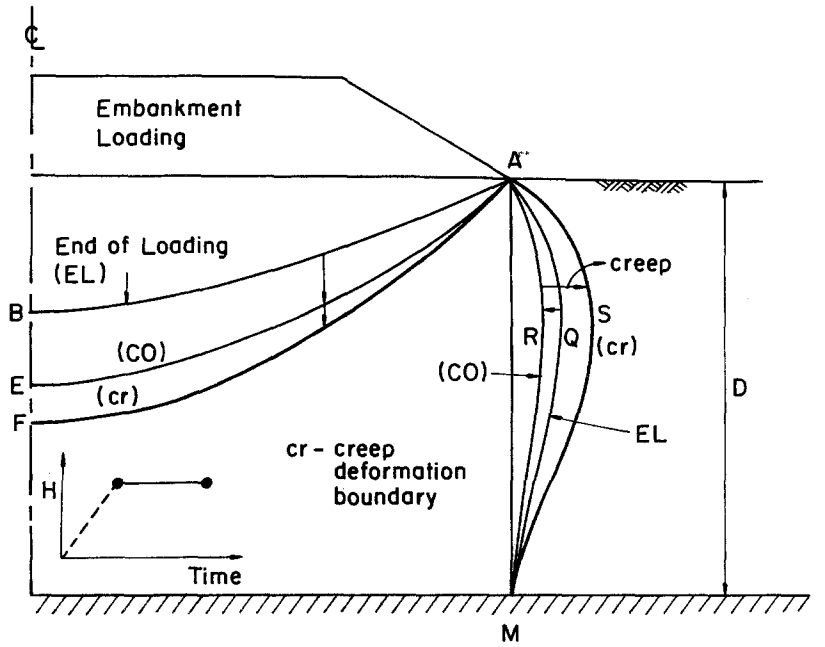

FIG. 4. Deformation Pattern of Embankment Foundation at End of Consolidation Stage

$$V_{hC} = \beta V_{crC} - \alpha V_{cC} \quad \ldots\ldots (15)$$

From (14) and (15), the volumetric deformation of the embankment foundation due to consolidation and creep can be written as in equations (16) and (17)

$$V_{cC} = \frac{\beta V_{vC} - V_{hC}}{\alpha + \beta} \quad \ldots\ldots (16)$$

$$V_{crC} = \frac{\alpha V_{vC} + V_{hC}}{\alpha + \beta} \quad \ldots\ldots (17)$$

In both normally consolidated and overconsolidated clays time dependent deformation due to creep can be quite large (Christian and Watt 1972). Since creep is a time-dependent parameter it can be assumed that

$$V_{crC} = Bxt^{\gamma} \quad \ldots\ldots (18)$$

where B and γ are constants. For different consolidation stages the constant B can be obtained as for loading stage

Stage j, $t = t_j$

$$B = \frac{\alpha\left[\frac{(V_{vC})_j}{t_j^{\gamma}}\right] + \left[\frac{(V_{hC})_j}{t_j^{\gamma}}\right]}{\alpha + \beta} \quad \ldots\ldots (19)$$

Stage $j + 1$, $t = t_{j+1}$

$$B = \frac{\alpha\left[\frac{(V_{vC})_{j+1}}{t^{\gamma}_{j+1}}\right] + \left[\frac{(V_{hC})_{j+}}{t^{\gamma}_{j+1}}\right]}{\alpha + \beta} \quad \ldots\ldots\ldots\ldots\ldots\ldots\ldots\ldots\ldots\ldots (20)$$

From (19) and (20) the ratio α can be evaluated as shown in (21)

$$\alpha = \frac{\left[\frac{(V_{hC})_{j+1}}{t^{\gamma}_{j+1}}\right] - \left[\frac{(V_{hC})_{j}}{t^{\gamma}_{j}}\right]}{\left[\frac{(V_{vC})_{j}}{t^{\gamma}_{j}}\right] - \left[\frac{(V_{vC})_{j+1}}{t^{\gamma}_{j+1}}\right]} \quad \ldots\ldots\ldots\ldots\ldots\ldots\ldots\ldots\ldots\ldots (21)$$

Coupling of drained creep in the analysis with the undrained creep is more cumbersome. Consideration of drained creep increases the number of unknowns and, thus, results in indeterminacy in the formulation of FDA. Therefore it was assumed that only undrained creep takes place in the field (i.e., $\beta = 1$).

Results

Initially, to establish the characteristics of Muar clay during construction, a 3-m-high and a 6-m-high control embankment, both of them constructed

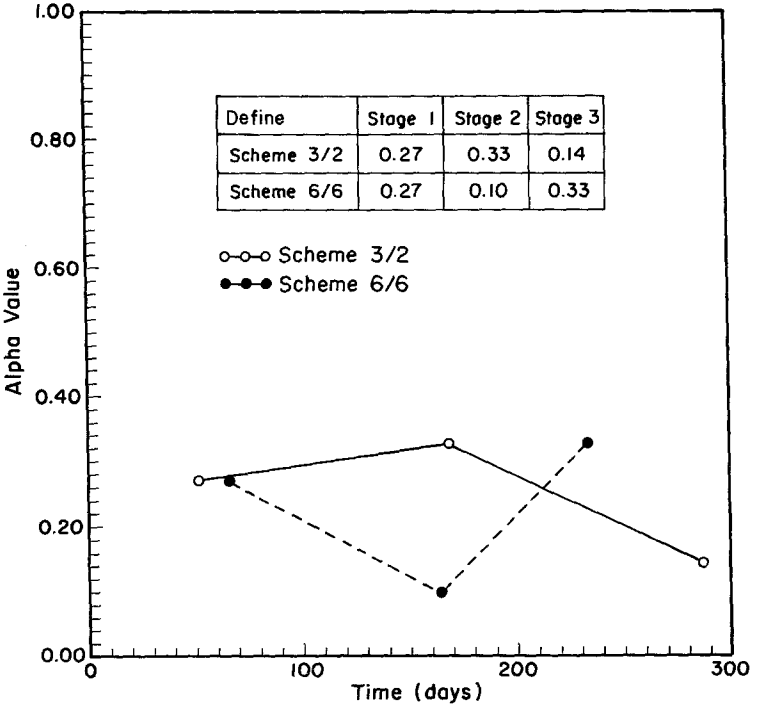

FIG. 5. α-Values for Different Stages of Construction

without any foundation ground improvement, were analyzed. The lateral volumetric deformation characteristics during loading were established by computing α values using (11). Fig. 5 shows the α values obtained for both the control embankments for different stages of loading, varies in the range of 0.10–0.32. The obtained α values revealed an average of 0.24, which represents an approximate unique volumetric deformation behavior of an embankment. The approximate volumetric deformation characteristics of the control embankments during loading stage due to undrained and consolidation processes was evaluated by substituting the average α value in (6) and (7), as follows:

$$V_{cL} = \frac{(V_{vL} - V_{hL})}{1.24} \quad \ldots\ldots (22)$$

$$V_{iL} = \frac{(0.24V_{vL} + V_{hL})}{1.24} \quad \ldots\ldots (23)$$

The values of V_{vL} and V_{hL} were calculated from the field settlement gauge and inclinometer measurements using (1) and (4). It was observed from the surface settlement profile, during different stages of loading, that the surface settlements (ρ) are uniformly related with the settlement volumes (V). These relationships for both 3 m and 6 m control embankments are given next

$$\text{3 m control embankment} - \rho = \frac{V}{12.5} \quad \ldots\ldots (24)$$

$$\text{6 m control embankment} - \rho = \frac{V}{23.0} \quad \ldots\ldots (25)$$

where ρ = the settlement at the centerline of the embankment. V = the settlement volume.

Using these linear relationships, for the loading stage, the immediate and the consolidation settlement components were obtained. The variation of immediate settlement and consolidation settlement are shown in Fig. 6. To obtain consolidation and creep settlement components separately, a similar analysis was performed for the consolidation stage. The variation of these two settlement components with time is shown in Fig. 7.

FINITE ELEMENT ANALYSIS (FEM) USING CRISP COMPUTER PROGRAM

The CRISP computer program, developed at University of Cambridge, was used for FEM analysis (Britto and Gunn 1987). Constitutive soil models included in this program are Cam-clay (both the original and the modified version), elastic perfectly plastic (options for von Mises, Tresca, Drucker-Prager, and Mohr-Coulomb models) and elastic isotropic and anisotropic models. This program allows undrained, drained, or fully coupled (Biot) consolidation analysis. The coupled consolidation model incorporates the undrained modified Cam-clay deformations and the drained consolidation settlements (Britto et al. 1987). The modified Cam-clay model, generalized by Roscoe and Burland (1968), is used in this analysis for foundation materials. This model was applied successfully for the prediction of MIT trial embankments (Wroth 1977) and the Malaysian test embankment (Balasubramaniam 1988).

Both the 3-m-high and 6-m-high control embankments were analyzed

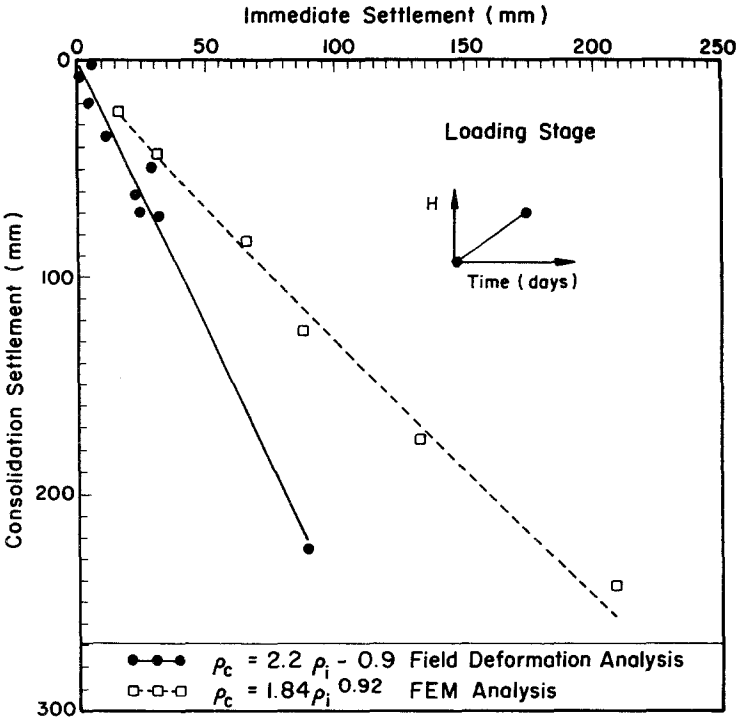

FIG. 6. Variation of Consolidation Settlement with Respect to Immediate Settlement

using CRISP. The finite element discretizations of these two embankments are shown in Figs. 8 and 9, respectively. Linear strain triangular (LST) elements were used. The aspect ratio of each element close to the loading area was maintained below 3. This condition was not strictly maintained for the elements away from the embankment loading area in order to minimize the computer time. The embankment loading was modeled as surface loading, since the analysis concerns only the settlement behavior. CRISP generates midside nodes of each element automaticaly in between the vertex nodes specified by the user.

Undrained Analysis

The immediate settlement component was calculated by performing undrained analysis. For undrained analysis element type number 2, linear strain triangle (LST) with displacement unknown was used. For undrained analysis pore fluid was considered as a separate material phase unlike in coupled consolidation analysis. In CRISP, the effective rigidity matrix $\mathbf{D}'$ is added to the pore fluid rigidity matrix $\mathbf{D}_f$ to form the total rigidity matrix $\mathbf{D}$. For drained analysis $\mathbf{D}'$ is, of course, equal to $\mathbf{D}$. For undrained analysis the term of $\mathbf{D}_f$ is computed from the bulk modulus of the water and void ratio. In CRISP the undrained behavior is modeled by assigning a value to k'/k_w in the range of 100 to 500, where k' = the bulk unit weight of soil and k'_w = the bulk unit weight of water. The range given for the ratio k'/k_w indirectly reflects the effects of the Poisson's ratio in the range from 0.49 to 0.499.

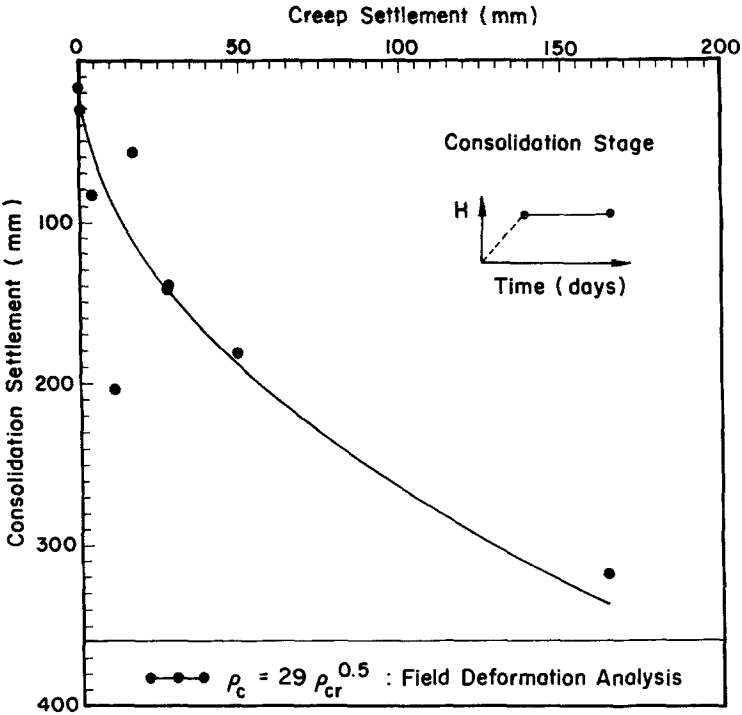

FIG. 7. Variation of Consolidation Settlement with Respect to Creep Settlement

Consolidation Analysis

The coupled consolidation analysis calculates total settlement during the loading and consolidation stages. The consolidation component is then separated by subtracting immediate settlement computed from undrained analysis. For consolidation analysis element type 3, LST with displacement and pore pressure unknown was used. The formulation of consolidation is based on Biot's three-dimensional consolidation theory, as described by Small et al. (1976). Physical nonlinearity is handled by dividing the applied load (and the time for consolidation analyses) into a number of increments and solving the system of equations using a tangent-stiffness approach. Since no iteration is performed, load and time must be kept small so that the stiffness coefficients, computed from the current effective stress state, can be considered appropriate for the increments.

Boundary Conditions

The following boundary conditions were used in the analysis, namely: (1) Lateral displacement is restricted in vertical ends; (2) lateral and vertical displacements are restricted along the bottom boundary; and (3) there is a free drainage boundary along the top surface.

Soil Parameters

Soil Parameters for the Malaysian Muar clay were obtained from field and laboratory tests ("3m high" 1988; Balasubramaniam 1989; Balachandran 1990). The input soil parameters used to perform analysis using CRISP

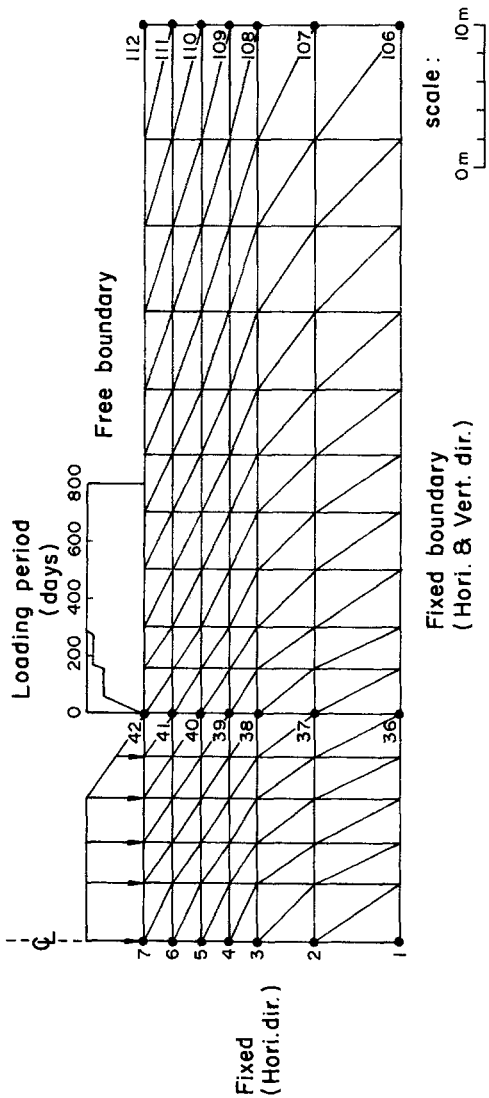

FIG. 8. Finite Element Discretization of 3-m-High Control Embankment

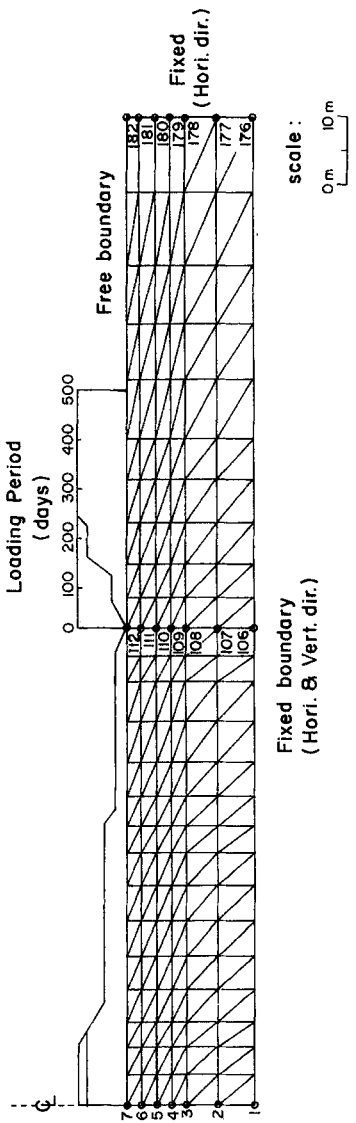

FIG. 9. Finite Element Discretization of 6-m-High Control Embankment

TABLE 1. Soil Parameters of Embankment Foundation (Modified Cam-clay Model): Undrained Analysis

Depth (m) (1)	κ (2)	λ (3)	e_{cs} (4)	M (5)	ν (6)	K_w (7)	γ_s (8)
0.0–2.0	0.05	0.13	3.06	1.19	0.3	4.440E4	16.5
2.5–8.0	0.05	0.13	3.06	1.19	0.3	1.115E4	15.5
8.0–18.0	0.08	0.11	1.61	1.07	0.3	2.270E5	15.5

TABLE 2. Soil Parameters of Embankment Foundation (Modified Cam-clay Model): Consolidation Analysis

Depth (m) (1)	κ (2)	λ (3)	e_{cs} (4)	M (5)	ν (6)	K_w (7)	K_h (m/s) (8)	K_v (m/s) (9)
0.0–2.0	0.05	0.13	3.06	1.19	0.3	16.5	1.5E-9	0.8E-9
2.5–8.0	0.05	0.13	3.06	1.19	0.3	15.5	1.5E-9	0.8E-9
8.0–18.0	0.08	0.11	1.61	1.07	0.3	15.5	1.1E-9	0.6E-9

TABLE 3. In Situ Stress Condition

Depth (m) (1)	$\bar{\sigma}_{x0}$ (kN/m^2) (2)	$\bar{\sigma}_{y0}$ (kN/m^2) (3)	U (kN/m^2) (4)	$\bar{P}_c$ (kN/m^2) (5)
0.0	0	0	0	110
2.0	13.24	22.0	16.68	110
8.0	33.73	56.11	75.54	40
18.0	67.87	113.11	173.64	60

are shown in Tables 1 and 2. Soil parameters required for the model can be obtained from standard oedometer and triaxial compression tests. These parameters are:

1. $\lambda = C_c/2.3$ = the gradient of the consolidation line in e-ln p' graph.
2. $\kappa = C_s/2.3$ = the gradient of the swelling line in the e-ln p' graph.
3. e_{cs} = the voids ratio at unit p' on the critical state line in the e-ln p' graph.
4. M = the value of the stress ratio q/p' at the critical state condition.
5. G = the elastic shear modulus of the soil.
6. k_v, k_h = the coefficients of permeability in vertical and horizontal directions used only for coupled consolidation analyses.

where:

$$p' = \frac{(\sigma_1' + 2\sigma_3')}{3} \quad \ldots\ldots (26)$$

and

$$q = (\sigma_1' - \sigma_3') \quad \ldots\ldots (27)$$

For the current study, the magnitude of λ was selected in such a manner

that the experimental undrained stress-strain curve coincides with the undrained predictions from the modified Cam-clay theory. Because intact undisturbed samples from the weathered crust were not recovered for laboratory testing, the Cam-clay properties of this topmost layer were assumed to be the same as those obtained for the silty clay layer just beneath it. Since the weathered crust is relatively thin (less than 2.0 m), the error caused by this assumption was anticipated to be small (Indraratna et al. 1992). In addition to these parameters the in-situ stress conditions are incorporated in the numerical analysis, including the in situ effective stesses (P_0'), isotropic preconsolidation pressure (P_c'), and the variation of ground-water pressures with depth as summarized in Table 3.

Analysis

Fig. 10 shows the variation of immediate settlement (at the centerline of the embankment base) with time, observed at the end of each loading stage obtained from FDA and FEM. During the initial stages when $t < 60$ days, the finite element analysis overestimates the immediate settlement when compared to FDA. This may be due to the underestimation of preconsolidation pressure in the laboratory. In CRISP, the preconsolidation pressure determines the initial yield conditions. Specifying low preconsolidation pressure leads to early yielding and thus higher settlements. Similar comparisons were made for consolidation settlement, as shown in Fig. 11. For $t < 30$ days, FEM overestimated settlement, and for $t > 30$ days FEM underestimated settlement when compared to FDA. The reasons for this observation may be: (1) The magnitude of λ selected in such a manner that the experimental undrained stress-strain curve coincides with the undrained predictions from the modified Cam-clay theory; and (2) the use of constant c_v value throughout the analysis, which may not concur with the actual field

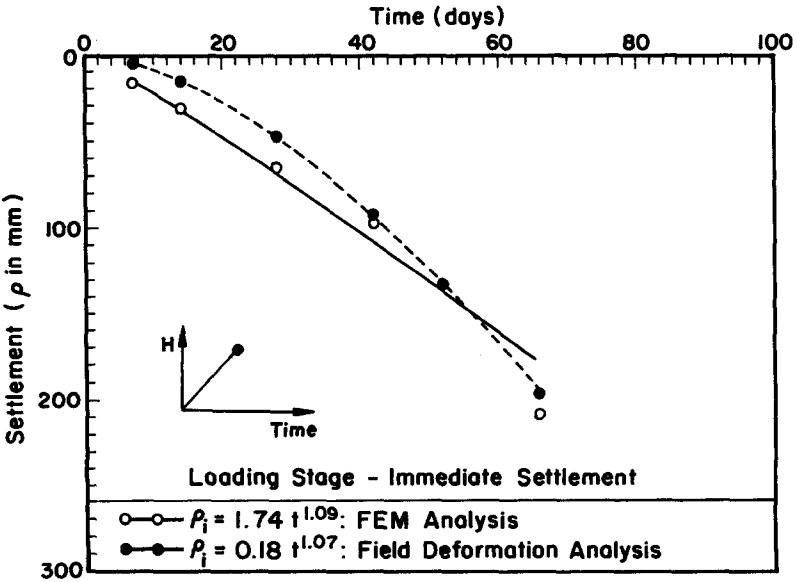

FIG. 10. Immediate Settlement versus Time (Loading Stage)

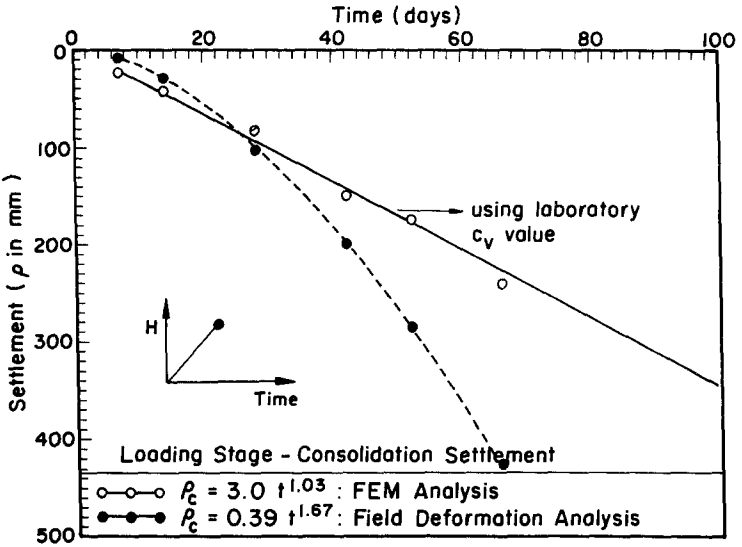

FIG. 11. Consolidation Settlement versus Time (Loading Stage)

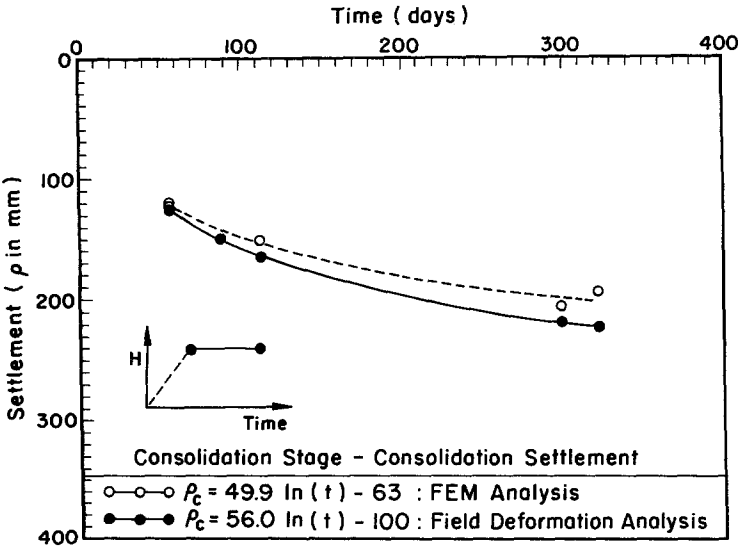

FIG. 12. Consolidation Settlement versus Time (Consolidation Stage)

condition, where c_v refers to consolidaton coefficient. The consolidation settlement components computed for consolidation stage, from FDA and FEM, are plotted against time, on Fig. 12, which show reasonably good agreement.

Immediate and consolidation settlements occur during the loading stage. These two settlement components were computed from field deformation analysis and finite element analysis separately. The consolidation settlement components computed were also plotted against immediate settlement com-

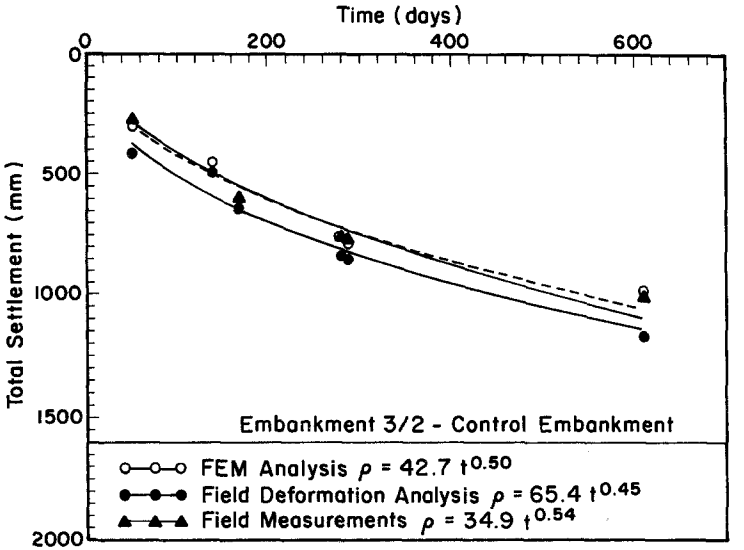

FIG. 13. Total Settlement with Time for 3-m-High Control Embankment

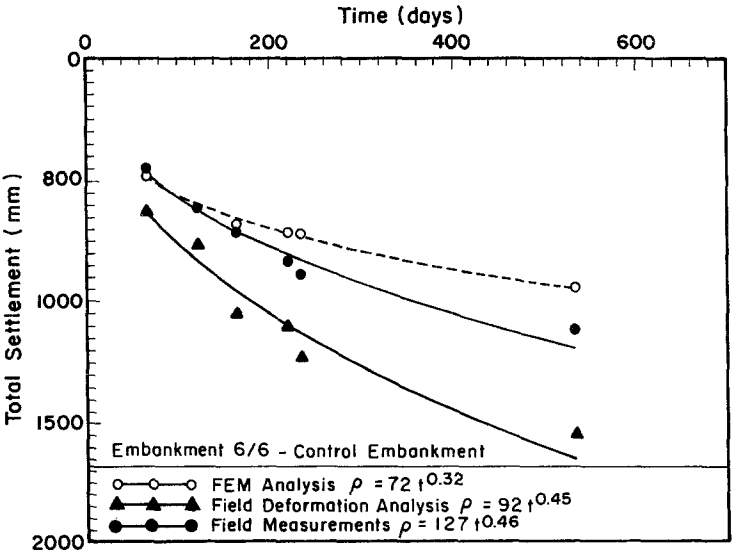

FIG. 14. Total Settlement with Time 6-m-High Control Embankment

ponents as shown in Fig. 6. The consolidation and the immediate settlement components vary as indicated next

$$\text{FDA} - \rho_c = 2.2\rho_i - 0.9 \quad \ldots\ldots (28)$$

$$\text{FEM} - \rho_c = 1.84\rho_i^{0.92} \quad \ldots\ldots (29)$$

where ρ_c represents consolidation settlement and ρ_i represents immediate

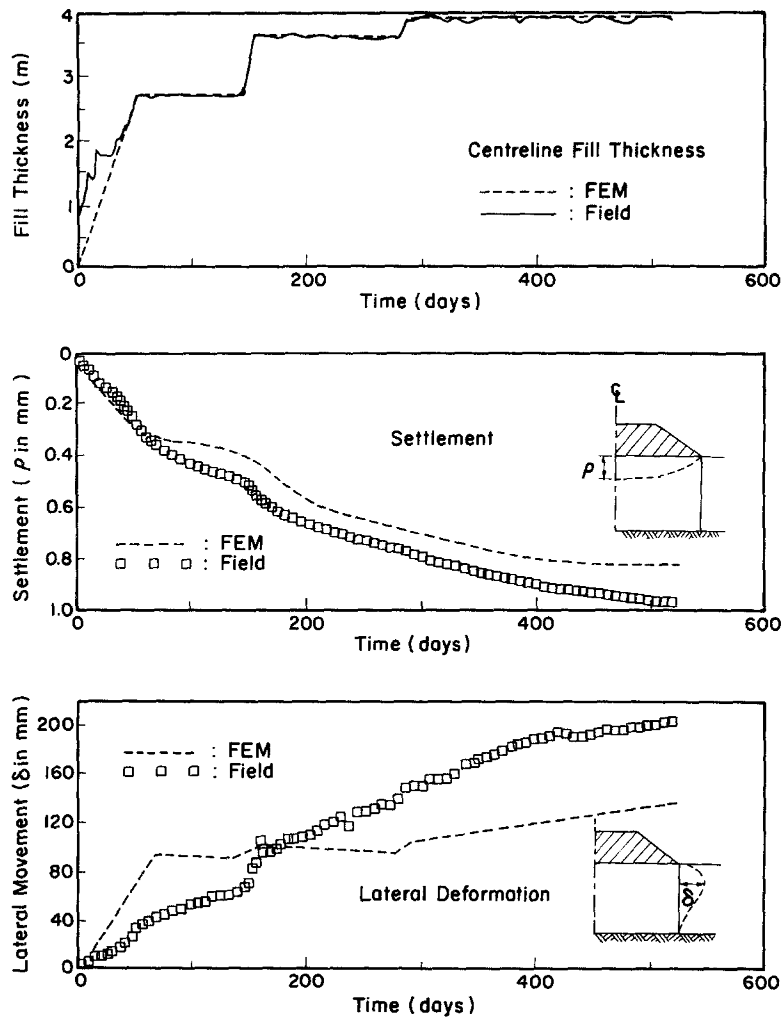

FIG. 15. Deformation Behavior of 3-m-High Control Embankment

settlement. These correlations were obtained by curve fitting technique (Fig. 6).

Consolidation and creep settlements occur during the consolidation stage. These settlement components are delineated from the total settlement observed using FDA. It is not possible to compute the time-dependent creep settlement components using CRISP, since the constitutive relation used is elasto-plastic. The variation of consolidation settlement with creep settlement (from FDA) is shown in Fig. 7. The nonlinear variation observed among these two components follows

$$\text{FDA} - \rho_c = 29\rho_{cr}^{0.5} \quad (30)$$

where ρ_{cr} represents the creep settlement.

The comparison of total settlements, for 3-m and 6-m control embank-

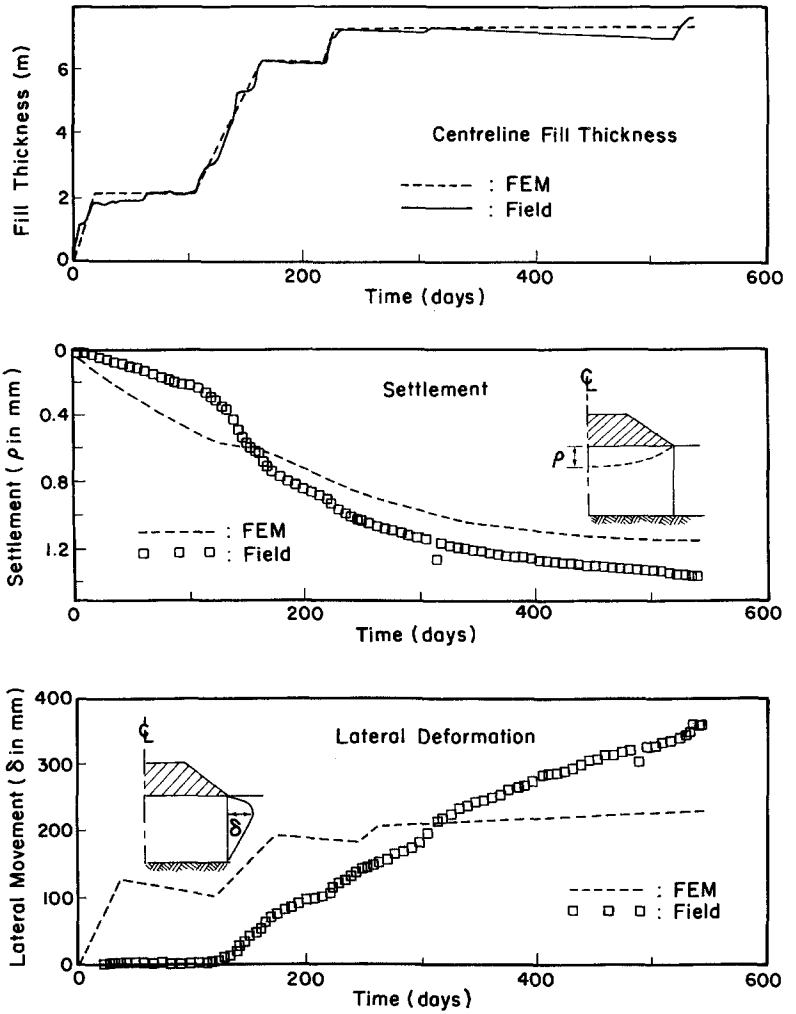

FIG. 16. Deformation Behavior of 6-m-High Control Embankment

ments, observed in the field, computed by FEM analysis and FDA is shown in Figs. 13 and 14. For the 3-m control embankment, FEM analysis predictions concur with the field observation. FDA overestimated the settlement by 100 mm. For the 6-m control embankment, FEM predictions are accurate for $t < 200$ days. For $t > 200$ days, FEM predictions underestimated the settlement. FDA overestimated the settlement from the beginning of construction and the overestimation was increasingly higher towards the end of the construction. Therefore, it can be concluded that FDA is a good tool in delineating and predicting settlement components for low embankments and for high embankments provided the period of construction is short.

The relationship between maximum lateral deformation and settlement beneath the center of an embankment is an indication of the embankment stability (Yamaguchi et al. 1984; Marche et al. 1974; Tavenas et al. 1978).

The lateral flow and settlement relationships for the 3-m-high and the 6-m-high control embankments, obtained from FEM analysis, are shown in Figs. 15 and 16, respectively. The field observations are also plotted for comparison. A linear relationship is observed between settlement and lateral deformation, at the end of the loading stages, as follows

$$\delta_{max} \sim 0.28\rho_{max} \quad \ldots\ldots (31)$$

where δ_{max} represents the maximum lateral deformation observed below the toe of the embankment and ρ_{max} represents the maximum settlement observed below the center of the embankment.

A similar observation was made by Suzuki (1988) as follows

$$\delta_{max} \sim 0.24\rho_{max} \quad \ldots\ldots (32)$$

It can be observed from Figs. 15 and 16 that, though settlement predictions concurred with field observations, the lateral deformations predicted were not accurate. The reasons attributed for this observation are: (1) The parameter λ used in CRISP is very sensitive in predicting the lateral deformations (Balachandran 1990) and therefore, a small error in the selection of appropriate λ value from laboratory testing results might have caused this difference; and (2) the analysis performed does not consider anisotropy of soil deformation parameters (e.g., G, λ, κ). In any case, there is no information from either laboratory or field tests on the Muar clay regarding this kind of anisotropy. Still et al. (1976) found that the effect of anisotropy in lateral deformation was very high at higher stress levels.

CONCLUSIONS

A new methodology, termed *field deformation analysis (FDA)* was applied to delineate and quantify different settlement components, namely: immediate settlement, consolidation settlement, and creep settlement from field-settlement observations. Subsequent comparison with results from finite element analyses indicate that immediate settlement was predicted with greater accuracy than consolidation settlement. Total settlement, obtained by adding the settlement components from FDA, is not representative in comparison with the total settlements observed in the field for long duration of construction period. This is because it was not possible to separate drained creep components due to the indeterminacy that arises in the formulation of FDA.

On step loading of an untreated embankment, during the loading stage, regardless of the loading rate and embankment dimensions, the consolidation settlement (ρ_c) was observed to vary almost linearly with the immediate settlement (ρ_i). The consolidation settlement was approximately twice the magnitude of the immediate settlement ($\rho_c = 2 - 2.2\rho_i$). Similarly, during the consolidaton stage, the consolidation settlement (ρ_c) was observed to vary with creep settlement (ρ_{cr}) nonlinearly as: $\rho_c = 29\rho_{cr}^{0.5}$.

Finite element method of analyses (FEM) coupled with critical state soil mechanics theory was performed to predict the deformation behavior of untreated embankments using the CRISP computer program. The results of finite element analysis indicated that the maximum lateral deformation beneath the toe of the embankment is approximately 0.28 times the maximum settlement observed below the center of the embankment at the end of loading stage.

ACKNOWLEDGMENTS

The writers wish to thank Mr. Robert Hudson, Dr. W. H. Ting, and Dr. E. W. Brand for their assistance in the clarifications of construction and testing details of Malaysian highway test embankments. The content of this paper is a part of the reseach work carried out by the first writer while he was a scholar of the government of Switzerland at the Asian Institute of Technology.

APPENDIX. REFERENCES

Balachandran, S. (1990). "Simulation of a test embankment failure (Muar flood plain, Malaysia) using finite element techniques coupled with critical state soil mechanics," ME thesis, Asian Institute of Technology, Bangkok, Thailand.

Balasubramaniam, A. S., Phin-wej, N., Indraratna, B., and Bergado, D. T. (1989). "Predicted behavior of a test embankment on a Malaysian marine clay." *Proc. Int. Symp. on Trial Embankments on Malaysian Marine Clays*, Kuala Lumpur, Malaysia, 2, 1(1)–1(8).

Brand, E. W., and Premchitt, J. (1989). "Moderator's report for the predicted performance of the Muar test embankment." *Proc. Int. Symp. on Trial Embankments on Malaysian Marine Clays*, Kuala Lumpur, Malaysia, 2, 1(32)–1(49).

Britto, A. M., and Gunn, M. J. (1987). *Critical state soil mechanics via finite elements*. Elis Horwood Limited.

Christian, J. T., and Watt, J. B. (1972). "Undrained visco-elastic analysis of soil deformations. Application of the FEM in Geotechnical Engineering." *Proc. Symp.*, Vickburk, Mississippi, May, 2, 533–574.

Harr, M. E., and Lovel, C. W. (1963). "Vertical stresses under certain axisymmetrical loading." *Highway Res. Board Record*, 39.

Indraratna, B., Balasubramaniam, A. S., and Balachandran, S. (1992). "Performance of test embankment constructed to failure on soft marine clay." ASCE 118(1).

Marche, R., and Chapuis, R. (1974). "Control of stability of embankments by the measurement of horizontal displacement." *Can. Geotech. J*, 11(1), 182–201.

Shibata, T. (1987). "Lateral deformation of clay foundations. Discussion Session 6." *Proc. 8th Asian Regional Conf. on S.M.F.E.*, Kyoto, 2, 390–391.

Small, J. C., Booker, J. R., and Davis, E. H. (1976). "Elastoplastic consolidation of soil." *Int. J. Solids Struct.*, 12, 319–326.

Stille, H., Fredriksson, A., and Broms, B. B. (1976). "Analysis of a test embankment considering the anisotrophy of the soil." *Numerical Methods in Geomechanics*, 2, June.

"3 m high control embankment on untreated soft ground." (1988). *Proc. Int. Symp. on Trial Embankments on Malaysian Marine Clays*, Kuala Lumpure, 2.

Suzuki, O. (1988). "The lateral flow of soil caused by banking on soft clay ground." *Soils Found.*, 28(4), 1–18.

Tavenas, F., Mieussens, C., and Bourges, F. (1978). "Lateral displacements in clay foundation under embankments." *Can. Geotech. J.*, 16, 532–550.

Ting, W. H., Chan, S. F., and Kassim, K. (1989). "Embankments with geogrid and vertical drains." *Proc. Int. Symp. on Trial Embankments on Malaysian Marine Clays*, Kuala Lumpur, 2.

Toh, C. T., Chee, S. K., Hudson, R. R., Loh, M. H., and Gue, S. S. (1989). "3 m high control embankment on untreated soft control ground. MHA." *Int. Symp. on Trial Embankments on Malaysian Marine Clays*, Kuala Lumpur, 2.

Wroth, C. P. (1977). "The predicted performance of soft clay under a trial embankment loading based on the Cam-Clay model." *Finite elements in geomechanics*, Gudehus, ed.

Yamaguchi, H. (1984). "Effect of depth of embankment on foundation settlement." *Soils Found.*, 24(1).